JACS
JOURNAL OF THE AMERICAN CHEMICAL SOCIETY
Article
pubs.acs.org/JACS

An Artificial Light-Harvesting Array Constructed from Multiple Bodipy Dyes

Raymond Ziessel,*[,†] Gilles Ulrich,[†] Alexandre Haefele,[†] and Anthony Harriman*[,‡]

[†]Laboratoire de Chimie Organique et Spectroscopies Avancées (ICPEES-LCOSA), UMR 7515 au CNRS, Ecole Européenne de Chimie, Polymères et Matériaux, Université de Strasbourg, 25 rue Becquerel, 67087 Strasbourg Cedex 02, France

[‡]Molecular Photonics Laboratory, School of Chemistry, Bedson Building, Newcastle University, Newcastle upon Tyne NE1 7RU, United Kingdom

Supporting Information

ABSTRACT: An artificial light-harvesting array, comprising 21 discrete chromophores arranged in a rational manner, has been synthesized and characterized fully. The design strategy follows a convergent approach that leads to a molecular-scale funnel, having an effective chromophore concentration of 0.6 M condensed into ca. 55 nm^3, able to direct the excitation energy to a focal point. A cascade of electronic energy-transfer steps occurs from the rim to the focal point, with the rate slowing down as the exciton moves toward its ultimate target. Situated midway along each branch of the V-shaped array, two chromophoric relays differ only slightly in terms of their excitation energies, and this situation facilitates reverse energy transfer. Thus, the excitation energy becomes spread around the array, a situation reminiscent of a giant holding pattern for the photon that can sample many different chromophores before being trapped by the terminal acceptor. At high photon flux under conditions of relatively slow off-load to a device, such as a solar cell, electronic energy transfer encounters one or more barriers that hinder forward progress of the exciton and thereby delays arrival of the second photon. Preliminary studies have addressed the ability of the array to function as a sensitizer for amorphous silicon solar cells.

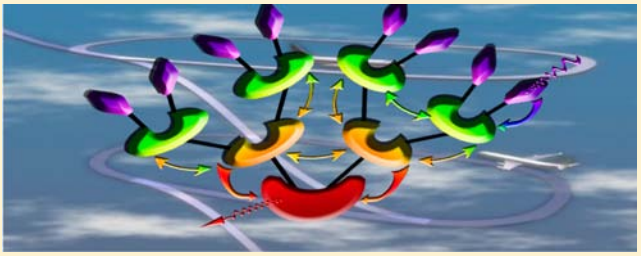

INTRODUCTION

The complex machinery of the photosynthetic apparatus found in higher plants serves two essential purposes, namely, to harvest sunlight and direct the resultant excitation energy to a reaction center[1] and also to provide protection against photochemical damage.[2] At first glance, these features appear to be mutually opposing! The collection of sunlight by artificial arrays is well documented,[3−5] and there are numerous descriptions of rationally designed molecular systems displaying efficacious intramolecular electronic energy transfer (EET). Additional attention has been given to the construction of plastic solar concentrators[6] and to the formulation of light-harvesting sensitizers[7] for use with specific types of solar cells. Much less attention, however, has been given to the problem of equipping such arrays with some form of self-protection against deleterious photochemical damage. In the natural system,[8] various mechanisms have evolved to ensure plant survival on those inevitable occasions when highly reactive intermediate species arise from exposure to a high photon flux. Such regulation of the light-harvesting machinery usually involves some kind of energy-dependent quenching,[9] although the details are still under active debate.[10] Incorporation of self-protection, however primitive this might be, is seen as an essential feature of any robust artificial system developed for solar energy conversion.[11] Otherwise, the array will not survive the harsh conditions associated with prolonged exposure of a sophisticated, multicomponent organic molecule to sunlight. Here, we describe an attempt to construct an artificial light-harvesting array able to dissipate excess photonic energy through a self-regulating mechanism. At the molecular level, the array is intended to collect photons over most of the visible range, terminating in a threshold wavelength appropriate for the sensitization of an amorphous silicon solar cell,[12] and channel the energy to an acceptor that can be anchored to a solid surface.[13] The capability to redistribute excess excitation energy is built into the system at an early stage. Further engineering of next-generation prototypes should ensure improved levels of photostability.

In designing the molecular array, we have relied heavily on prior work[14−16] using the boron dipyrromethene (Bodipy) family of highly fluorescent dyes. Such materials, possessing triplet quantum yields well below 5% in the absence of spin orbit perturbation, have been exploited for numerous photonic devices, including cascade energy-transfer processes,[17] flow cytometry,[18] protein labeling,[19] cell internalization,[20] biolabeling,[21] chemical probes,[22] and two-photon imaging.[23] The facile chemical modification of the generic Bodipy framework[24] provides the impetus to construct elaborate molecular architectures, whereby selected dyes can be arranged in a

Received: May 27, 2013
Published: July 3, 2013

   dx.doi.org/10.1021/ja4049306 | J. Am. Chem. Soc. 2013, 135, 11330−11344

logical sequence and where the optical properties of individual dyes can be fine-tuned[25] for particular purposes. A key discovery[26] in this field relates to the replacement of the conventional B−F bonds with B−C analogues since this permits the attachment of a multitude of disparate functionalities and diversification of the dimensionality of the construct. The "chemistry at boron" approach[27] has been applied here to covalently attach a total of 20 ancillary chromophores (including 6 tolane linkers) to the terminal acceptor, thereby producing a cascade-type molecular array capable of directed EET (Chart 1). The gradient of excitation energies is intended

Chart 1. Molecular Formula of the Target Array Comprising Eight Pyrene Units (Grey), Attached in Pairs to Four Tetramethyl-Bodipy Dyes (Green) That Are Bundled in Pairs to Two Fully Alkylated Bodipy Dyes (Orange) That Are Linked to the Terminal Expanded Bodipy Dye (Blue)[a]

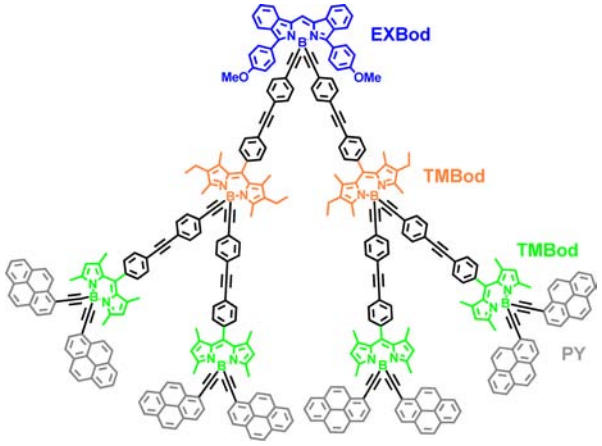

[a]Note the use of tolane spacer units to separate the various Bodipy dyes. There is an excitation energy gradient running from pyrene to the expanded Bodipy dye. See Figure S1 for a 3D representation of the cluster as generated by molecular dynamics simulations.

to facilitate EET from the outermost pyrene (PY) to the expanded Bodipy (EXBod), with the intermediate dyes functioning as energy relays. The mechanism for each EET step, that is, the distinction between through-bond or through-space interactions, is not important in the present context, but the overall EET efficiency is critical.

The design principle is based on the exciton blockade approach introduced some years ago,[28] this being a derivative of the better known coulomb blockade recognized in low-temperature physics.[29] The general idea is that, under intense illumination, several excitons will be added to the light-harvesting array and will migrate toward the terminal acceptor. Energy transfer to the latter might be restricted if it is already in an excited state (i.e., the rate of EET depends on the state of excitation of the terminal acceptor). As such, a key feature of the molecular topology is to provide diverse routes for the exciton that will ensure disparate arrival times. It might be argued that such behavior is best examined at the single-molecule level where light intensities can be varied dramatically.[30] There have, in fact, been several studies of the exciton blockade carried out with single-molecule dendrimers,[31] but the impact of conformational heterogeneity prevents unambiguous recognition of the effect. Structural distortions that fluctuate on the nanosecond time scale[32] are always likely to interfere with data analysis in elaborate multicomponent molecular arrays[33] and must be considered during data interpretation.

Perhaps it is instructive to draw attention to other molecular arrays that display cascade-type EET, neglecting linear dyads and triads. The most relevant architectures are dendrimers,[34] and there are numerous such entities able to direct excitons from the periphery to the core by way of successive EET steps.[35] These dendritic frameworks can be flexible[36] or semirigid,[37] and because of their topology, EET does not need to follow a single branch. Indeed, energy hopping between branches could serve to distribute the excitation energy around the dendrimer before being localized at the central unit.[35] Conjugated polymers also provide facile means for both inter- and intrastrand EET[38] that lead to widespread redistribution of energy throughout the matrix. Advantages of the cluster described herein are that the terminal energy acceptor is readily available for anchoring to a surface where the exciton can be off-loaded, easy control of the rates of EET via slight modification of the bridging units, and simple tuning of the optical properties so as to meet any desired threshold wavelength (e.g., sensitization of a particular semiconductor). Other strategies, such as dye-decorated platforms[39] or self-assembly of heterodyes[40] should also be considered. All such architectures, where multiple dyes are brought into close proximity, are likely to exhibit nonlinear optical behavior in respect to incident photon densities.[41] Again, it should be stressed that single-molecule approaches[42] offer obvious advantages for attaching several photons to a solitary array.

RESULTS AND DISCUSSION

Design and Synthesis. The target molecular entity is intended to serve two functions; namely, (i) the collection of photons over a wide spectral window, with subsequent channeling of the excitation energy to a single site, and (ii) the dissipation of excess photonic energy by way of harmless processes. The first requirement leads to the design of a molecular funnel comprising a series of closely spaced chromophores graded so as to favor a cascade of EET steps leading to a stable fluorescent species. Many such systems are known,[43] and we have opted to use Bodipy building blocks for most of the construction work. The second requirement, being essentially unknown in artificial systems but being an integral part of all natural photosystems,[8] is much more demanding. Our approach to this problem involves using a pair of chromophores for which the individual energy levels are sufficiently similar for the respective excited states to establish a thermal equilibrium.[44] The final design links 21 chromophores in an ordered array; individual units being 8 ethynylpyrene (PY) residues, 4 tetramethyl-Bodipy (TMBod) dyes, 2 tetramethyldiethyl-Bodipy (MEBod) dyes, 6 tolane functions, and an expanded Bodipy (EXBod) dye as the terminal acceptor. The most logical strategy by which to construct such an edifice is to use a convergent protocol[45] whereby the peripheral chromophores are introduced early in the synthesis. A critical feature of this approach concerns the need to provide for adequate solubility and characterization at each stage of evolution so that the stoichiometry can be assured.

Isolation of the two conventional Bodipy-based synthons involved similar but not identical protocols. Thus, the tetramethyl-Bodipy analogue **3** was prepared in three steps, starting with selective substitution at the B−F bonds using a Grignard reagent obtained from 1-ethynylpyrene and leading to isolation of compound **2**. This was followed by functionaliza-

dx.doi.org/10.1021/ja4049306 | J. Am. Chem. Soc. 2013, 135, 11330−11344

Scheme 1[a]

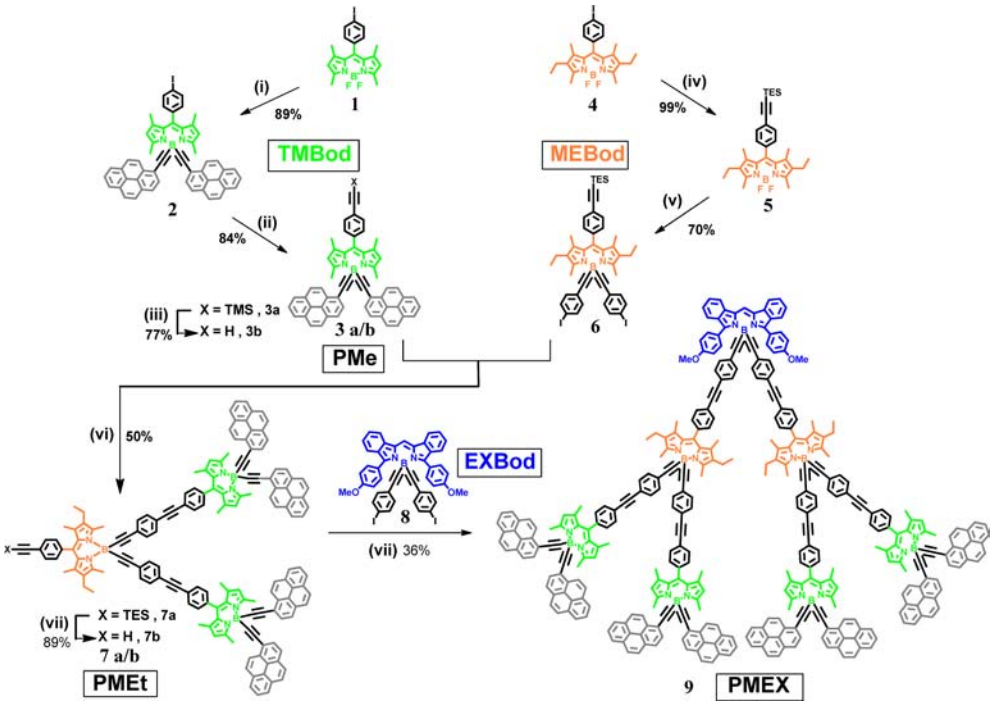

[a]Key: (i) 1-ethynylpyrene, EtMgBr, THF, 60 °C; (ii) trimethylsilylacetylene, $[Pd(PPh_3)_2Cl_2]$ (6 mol %), CuI (10 mol %), diisopropylamine, THF, rt; (iii) KOH, MeOH, H_2O, rt; (iv) triethylsilylacetylene, $[Pd(PPh_3)_2Cl_2]$ (6 mol %), CuI (10 mol %), di-isopropylamine, THF, rt; (v) 1-ethynyl-4-iodophenyl, EtMgBr, THF, 60 °C; (vi) compound **3** (2 equiv), compound **6** (1 equiv) $[Pd(PPh_3)_4]$ (6 mol %), triethylamine, benzene, 60 °C; (vii) $[Pd(PPh_3)_4]$ (2 mol %), triethylamine, benzene, 60 °C.

tion of the iodo-group using trimethylsilylacetylene and deprotection with a mineral base, thereby affording compound **3b** in an overall yield of 58% (left-hand side of Scheme 1). Also straightforward is the preparation of synthon **6** by a sequence of reactions starting by cross coupling with triethylsilylacetylene. This latter reaction was promoted by Pd(0) complexes and led to isolation of compound **5**. This was followed by reaction with the Grignard reagent formed from 1-ethynyl-4-iodobenzene, thereby affording derivative **6** in an overall yield of 70% (right-hand side of Scheme 1). The final step involves cross-coupling 2 equiv of **3b** with 1 equiv of **6** using a Pd(0) complex in the absence of copper salts and molecular oxygen. The pivotal intermediate **7a** was isolated as a pure sample in excellent yield by standard separation techniques (see Supporting Information).

The final, and indeed critical, step consists of cross coupling 2 equiv of module **7b** (PMEt) with the terminal acceptor **8**. The major difficulty here is to circumvent the strong tendency of **7b** to form the homocoupled compound (i.e., the butadiyne-bridged derivative). This type of reaction is usually promoted by copper salts[46] but can be catalyzed also with palladium salts in specific cases.[47] To find ways around this undesirable side reaction, many different experimental conditions were tried; these included changes in solvent, base, catalyst, concentration, and temperature. On the basis of these studies, it appears that the use of a low concentration of catalyst and the strict avoidance of copper salts provides the best conditions for isolation of the target dye in acceptable yield (Scheme 1).

All intermediates and target compounds were analyzed by proton NMR spectroscopy, and a selection of relevant spectra is given in Figure 1. For compound **3b**, for example, the presence of a singlet for both β-pyrrolic protons at 6.2 ppm, which integrates for two protons, compared to the doublet at 8.8 ppm (integration for two protons) belonging to the pyrene units allows us to conclude that double substitution has occurred at the boron center (Figure 1). Interestingly, the spectrum of compound **7b** resembles a linear combination of spectra for compounds **3b** and **6** without notable overlapping between respective peaks. In particular, integration of the ethyl peaks compared to the methyl peaks of dyes **6** and **3b** confirms that double substitution of both iodo-groups has taken place. This situation was confirmed subsequently by the MALDI-TOF MS spectrum that exhibits a molecular peak at 2087.0/2086.0 amu, with an isotopic profile in agreement with the calculated spectrum.

The well-defined NMR spectrum found for the final compound **9** is also quite informative (Figure 2). The methoxy signal for this terminal blue dye indicates that both iodine moieties present in **8** have been replaced with the intended modules. In particular, integration of this methoxy signal (singlet at 3.8 ppm with integration for 6 protons) perfectly matches the 8-proton integration of the β-pyrrolic signal belonging to the incoming four-component module **7b**. Further confirmation is provided by the 4-proton integration of the doublet at 7.05 ppm belonging to the AB quartet of the anisole fragment of the blue dye which matches the expected 8 protons (localized at the ortho position of the alkyne) for 8 pyrene residues at 8.8 ppm (Figure 2). Confirmation of the molecular composition of the final dye is provided by the MALDI-TOF MS spectrum that exhibits a molecular peak at 4836.8/4837.8 amu, with an isotopic profile in agreement with the calculated spectrum. Treating the edifice as a cone of height 48 Å and radius 33 Å containing 21 chromophores leads to an estimate for the effective pigment concentration as being ca. 0.6 M. The

dx.doi.org/10.1021/ja4049306 | J. Am. Chem. Soc. 2013, 135, 11330−11344

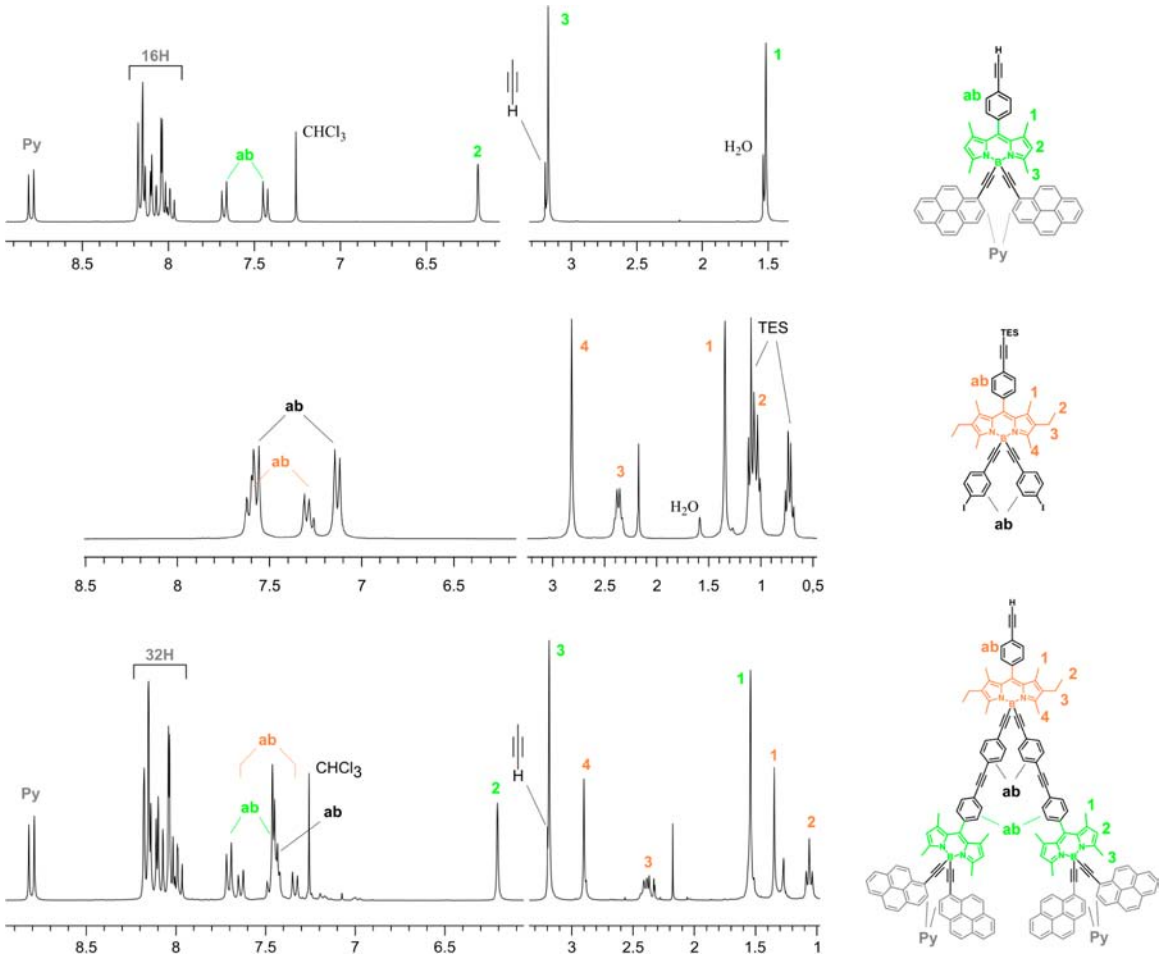

Figure 1. Proton NMR spectra of the key model compounds **3b**, **6**, and **7b** from top to bottom, recorded in $CDCl_3$ at 300 MHz.

threshold wavelength for absorbing sunlight is ca. 670 nm, this being appropriate for sensitization of amorphous silicon solar cells, and with the target cluster dispersed in a plastic matrix, ~30% of the solar spectrum can be harvested without self-absorption or concentration quenching. This is a marked improvement on conventional plastic solar concentrators.[6]

Photophysical Investigations. The starting point for this investigation lies with exploring EET from 1-ethynylpyrene (PY) to the appended TMBod derivative, taking note that two PY units are attached to the dye by way of the boron center. Similar molecular dyads have been studied before,[48] having various aryl polycycles attached to the boron atom (or meso-carbon), and it has been established that EET from polycycle to Bodipy is rapid and essentially quantitative. The same situation is found for **3b** (hereafter abbreviated as PMe for simplicity) in 2-methyltetrahydrofuran (MTHF) at room temperature. Thus, the absorption spectrum (Figure 3) indicates that the TMBod chromophore exhibits pronounced absorption bands with a maximum at 501 nm and a vibronic progression stretching toward higher energies. Absorption transitions localized on PY are seen as a series of well-resolved bands in the wavelength range 300−390 nm. These latter transitions overlap with higher-energy absorption bands associated[49] with TMBod. Excitation into the PY unit at around 365 nm leads to the appearance of strong fluorescence with a maximum at 518 nm that is characteristic of TMBod (Figure 3); the same spectral profile is observed following illumination at 470 nm, where only TMBod absorbs. The excitation spectrum matches well with the absorption spectrum over the entire spectral window, and it is clear that photons collected by PY are transferred quantitatively to TMBod under these conditions. Both the fluorescence quantum yield (Φ_F = 0.78 ± 0.03) and the excited-state lifetime (τ_S = 4.6 ± 0.1 ns) recorded for TMBod remain independent of excitation wavelength. In addition, the time-resolved fluorescence decay profiles obtained after excitation at 310, 470, or 490 nm are monoexponential. These Φ_F and τ_S values are unexceptional[50] for a conventional Bodipy dye.

For PMe in MTHF it was not possible to resolve fluorescence characteristic of PY from the baseline, even in a glassy matrix at 77 K. Emission from the pyrene unit is expected over the region 430−500 nm and will overlap with absorption by the Bodipy chromophore (Figure S2). Unlike the situation with other pyrene-Bodipy dyads,[25c] the absorption spectral profile for PMe favors EET to the first-excited singlet state resident on TMBod. Comparison to a 2:1 molar mixture of 1-ethynylpyrene and **1** in MTHF led to the conclusion that the level of quenching of the excited-singlet state of the PY unit present in PMe exceeds 99.5% while, on the basis of time-resolved emission studies, the PY fluorescence lifetime is <10 ps (cf τ_S of 3.0 ns for 1-ethynylpyrene).[50] The center-to-center separation distance is ca. 8.5 Å, while the connection at the pyrene terminal is likely to favor through-bond EET.[51] Consequently fluorescence quenching is attributed to intra-molecular EET, as has been reported for many related dyads[25]

dx.doi.org/10.1021/ja4049306 | J. Am. Chem. Soc. 2013, 135, 11330−11344

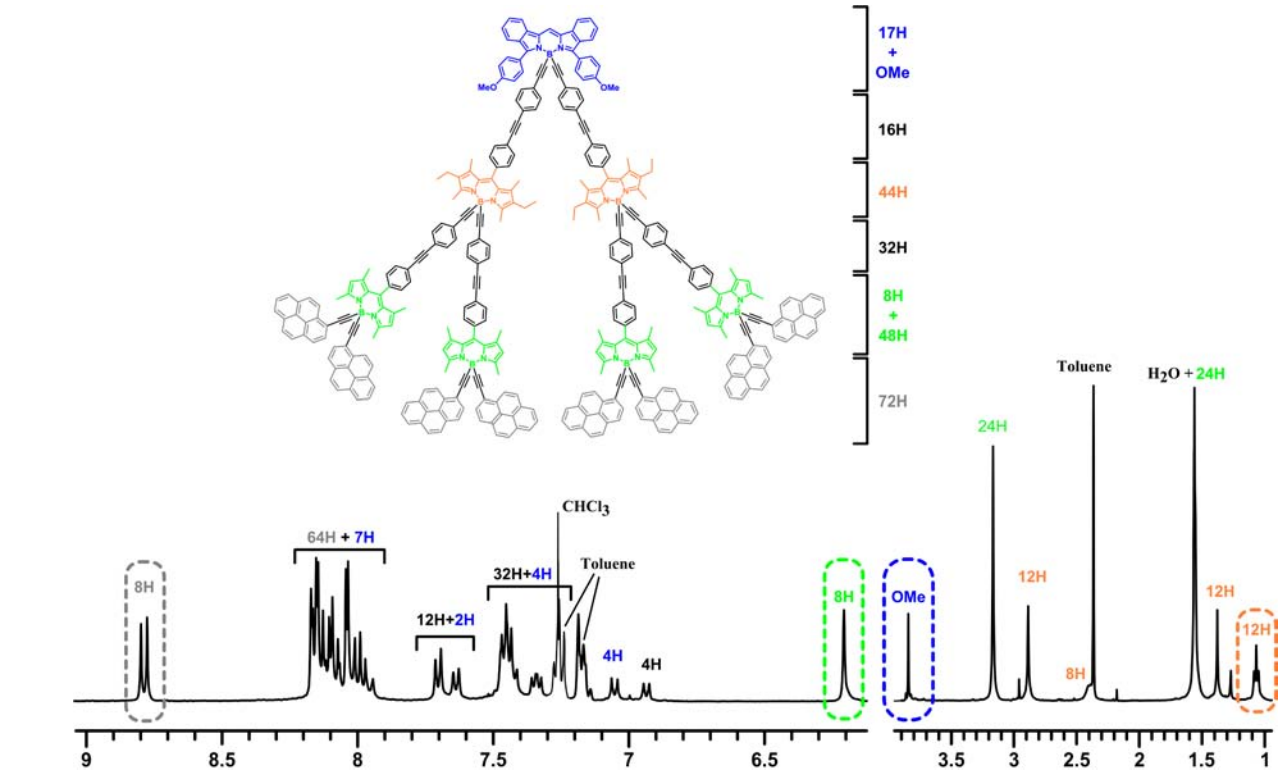

Figure 2. Proton NMR spectra of the key model compound **9** recorded at room temperature in $CDCl_3$ at 400 MHz.

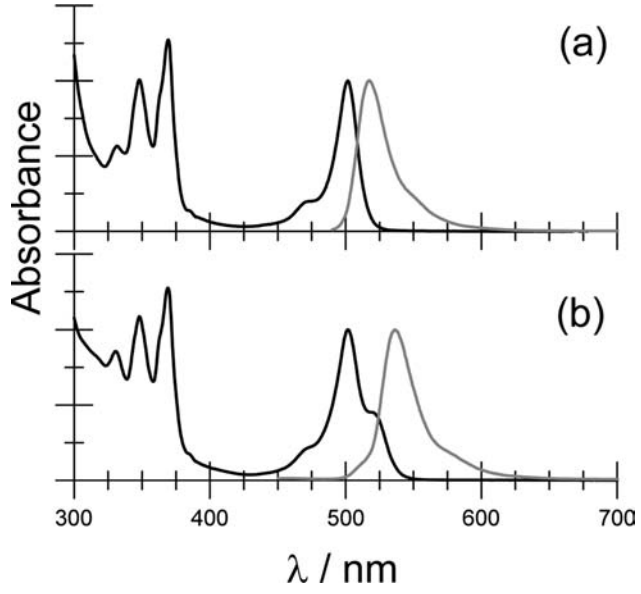

Figure 3. Normalized absorption (black curve) and fluorescence (gray curve) spectra recorded for (a) PMe (**3b**) and (b) PMEt (**7b**) in MTHF at room temperature. The excitation wavelength was 365 nm.

and used[15] to extend the Stokes' shift for Bodipy-based fluorescent labels.

Turning attention now to **7b** (hereafter abbreviated PMEt for simplicity) where the additional Bodipy residue has been added, we note that in structural terms the new fluorophore differs from TMBod only by the presence of two ethyl groups on the dipyrrin nucleus; we will refer to this new dye as MEBod to signify the presence of both methyl and ethyl functions. These ethyl groups push the absorption maximum from 501 to 522 nm in MTHF at room temperature.[14] The individual Bodipy-based transitions can be resolved in the absorption spectrum, although the stoichiometry has to be taken into account when considering the relative intensities (Figure 3). Notice should also be given to the arrangement of these dyes and, in particular, their proximity to the PY unit which will serve as the principal excitation point for EET studies. Thus, following illumination at 365 nm, the fluorescence spectrum shows no indication for emission from the PY unit but exhibits two overlapping fluorescence profiles with maxima at 518 and 540 nm (Figure 3). This dual emission can be attributed to fluorescence from both TMBod and MEBod, although the ratio is clearly in favor of the latter when due allowance is made for the relative Φ_F values.[52] Excitation spectra recorded for emission at 600 nm confirm that photons absorbed by both PY and TMBod units lead to emission from the MEBod fluorophore (Figure S3). Excitation into TMBod at 475 nm gives rise to the same dual emission profile as observed on illumination into PY. Consequently, we can conclude that intramolecular EET occurs from TMBod to MEBod in the array. Deconvoluting the spectral profile into components associated with TMBod and MEBod, spectra being available for the reference compounds, indicates the former accounts for only 7% of the total fluorescence signal (Figure S4).

The control compound for MEBod, namely **4**, shows strong fluorescence in MTHF at room temperature. Here, $\Phi_F = 0.75 \pm 0.03$, while $\tau_S = 4.8 \pm 0.2$ ns; these values being normal[14] for a conventional Bodipy dye. Time-resolved fluorescence studies indicate that τ_S for the MEBod residue present in PMEt is reduced slightly to 4.5 ± 0.2 ns; fluorescence quantum yields for MEBod and PMEt (λ_{EX} = 515 nm) are within ±8%. There is no suggestion that the slight shortening of the lifetime is indicative of (e.g., electron transfer) quenching in the array, and instead we attribute this minor effect to some kind of geometric distortion introduced at the S_1 level by imposing bulky

dx.doi.org/10.1021/ja4049306 | J. Am. Chem. Soc. 2013, 135, 11330−11344

substituents at the boron atom.[17f] Somewhat surprisingly, emission from the TMBod unit in PMEt also decays with this same lifetime, no matter how carefully this measurement is made with respect to excluding fluorescence from MEBod. Close spectral overlap between the two fluorescence profiles, together with a small amount of hot fluorescence if excitation is made in the near-UV region, means it is difficult to completely exclude emission from MEBod when examining the region associated with TMBod; the best interrogation wavelength is 510 nm (Figure S5).

In this regard it is important to note that the fractional contribution made by TMBod emission increases slightly with increasing temperature over the range 255−385K (Figure 4),

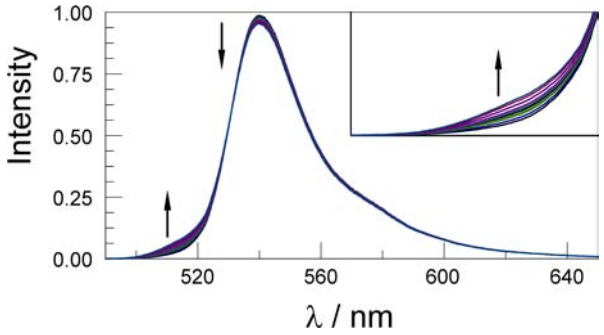

Figure 4. Effect of increasing temperature on the fluorescence spectrum recorded for PMEt (7) in MTHF; the insert shows an expansion of the wavelength range from 500 to 520 nm.

thereby indicating that the two emitting species are in thermal equilibrium[44] over this region. Assuming the ratio of the fluorescence yields is set by the Boltzmann distribution law, the energy gap between the two states is estimated to be 700 cm^{-1} (i.e., 8.4 kJ/mol). This can be compared with the spectroscopic energy gap of 795 cm^{-1} derived from absorption and emission spectra of the reference compounds. In turn, the calculated energy gap can be used to estimate the equilibrium constant, K = 0.04, at room temperature.

Measurement of the rate of intramolecular EET from TMBod to MEBod was not straightforward because of the significant overlap between fluorescence from the two Bodipy residues (Figure S5). Thus, it proved difficult to isolate emission from either of these dyes without contamination from the second dye. In principle, the required level of resolution might be expected from frequency-domain measurements made with phase modulation techniques, but this was not so. Here, the problem was poor sensitivity, although the lifetime of the MEBod (τ_S = 4.5 ± 0.3 ns) could be recovered on excitation into either PY at 310 nm or one of the Bodipy dyes at 490 nm.

More reliable results were obtained by time-correlated, single photon counting with excitation at 340 nm delivered from a picosecond laser diode (average power 1 mW at 40 MHz) and with detection via a cooled microchannel plate PMT. The instrument response function recorded under optimized conditions was <70 ps. Analysis with iterative reconvolution of emission from the TMBod unit indicated that decay occurs via dual-exponential kinetics. The shorter-lived component,[53] accounting for ca. 90% of the total signal, gave a consistent estimate for τ_S of 35 ± 6 ps (Figure 5). The slower component required analysis on much longer time scales but was found to correspond to a lifetime of 4.0 ± 0.6 ns. Monitoring at longer wavelength showed that emission associated with MEBod

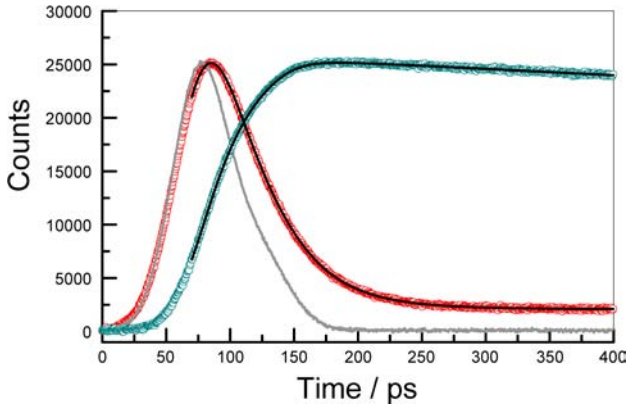

Figure 5. Time-resolved emission profiles recorded for PMEt in MTHF at room temperature following excitation at 340 nm. The IRF is shown as a gray curve, while fluorescence from TMBod at 510 nm is shown as a red curve with the fit (χ^2 = 1.09) is superimposed as a black curve. Growth of fluorescence from MEBod at 590 nm is shown as a blue curve with the fit (χ^2 = 1.24) superimposed as a black curve. See Figure S6 for a plot of the weighted residuals.

grows-in with a time constant of 39 ± 5 ps but barely decays over several hundred ps. Global analysis across the 500−600 nm window was consistent with a reaction scheme whereby the excited-singlet state of TMBod decays with a lifetime of ca. 40 ps to populate the corresponding excited-singlet state resident on MEBod with the same time constant (Figure 6).

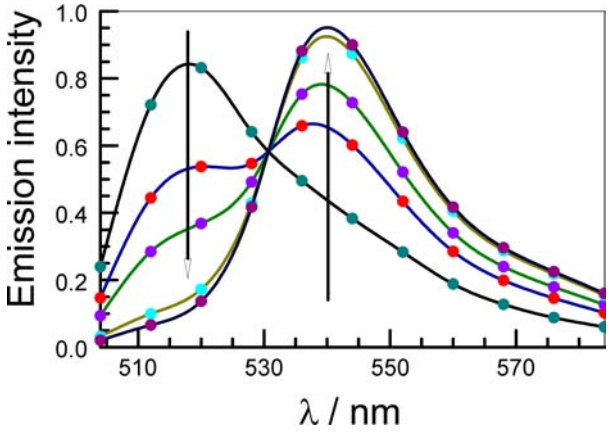

Figure 6. Time-resolved fluorescence spectra recorded for PMEt in MTHF at room temperature following excitation at 340 nm. Spectra were compiled at 25 (blue), 40 (red), 65 (lilac), 145 (light blue) and 225 ps (plum).

It should be recalled that the temperature dependence noted above indicates that these two excited-singlet states are in thermal equilibrium under ambient conditions. Effectively, this situation corresponds to E-type delayed fluorescence.[54] Now, in the simplest case, the inverse of τ_S can be equated to the sum of the forward and reverse EET rate constants, while the equilibrium constant represents the ratio of these two rate constants. This simplified scheme allows derivation of the rate constants for forward (TMBod* → MEBod) and reverse (MEBod* → TMBod) EET steps as being 2.4 × 10^{10} and 1.0 × 10^9 s^{-1}, respectively, at 295 K. The thermally equilibrated mixture of excited-singlet states decays with a common lifetime of ca. 4 ns.

dx.doi.org/10.1021/ja4049306 | J. Am. Chem. Soc. 2013, 135, 11330−11344

Because of the molecular topology, reverse EET in PMEt could populate the S_1 state associated with either of the two TMBod units. In this way, the photonic energy migrates around the array and samples all three Bodipy-based chromophores. Through-space (i.e., direct) EET between the two TMBod units is unlikely because of the extended separation distance, estimated from computer-generated molecular models[55] to be ca. 29 Å and limited spectral overlap integral.[56] On the assumption that this particular EET step occurs exclusively via Förster dipole−dipole coupling,[57] the critical distance (R_{CD}) for EET between TMBod molecules held in random orientation can be computed from spectroscopic data to be 20.5 Å. As such, we estimate the rate constant for through-space EET between TMB units as being ca. 3.0×10^7 s^{-1}. This can be compared to the rate constant ($k_{EET} = 2.4 \times 10^{10}$ s^{-1}) for EET from TMBod to MEBod, where the separation distance is 18.0 Å and where the mechanism is most likely dominated by through-bond interactions.[27] At best, energy migration between the two TMBod units, therefore, will account for ca. 1% of the initial excitation energy, but this will be supplemented by reverse EET from MEBod; see Figure S7 for a reconstruction of the steady-state fluorescence spectrum based on the derived photophysics. It is important to note that the rate constant (k_{REET}) for reverse energy transfer from the excited-singlet state of MEBod to TMBod has a value of 1.0×10^9 s^{-1} and is therefore competitive with inherent deactivation of the exciton (see Figure S8 for a distribution profile based on solving the appropriate ordinary differential equations).

Continuing along the projected EET axis, the photophysics of **9** (hereafter abbreviated as PMEX for simplicity) were studied in CH_2Cl_2; this compound being poorly soluble in MTHF at ambient temperature. The absorption spectrum (Figure 7) shows the presence of a rich variety of transitions

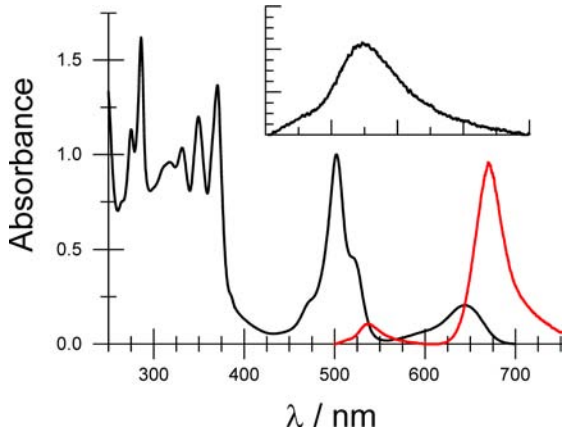

Figure 7. Absorption (black curve) and fluorescence (red curve) spectra recorded for PMEX (**9**) in CH_2Cl_2 at room temperature. The excitation wavelength was 365 nm. The insert shows an expansion of the emission spectrum over the range 500−600 nm.

which are easily explained in terms of the earlier description. Thus, the terminal acceptor, EXBod, which is a class of expanded Bodipy dyes,[58] has an absorption maximum located at 645 nm and is clearly visible on the low-energy side of the spectrum. This optical transition is broader than those found for conventional Bodipy dyes but comparable to spectra reported[59] for related dyes in solution. The familiar patterns for the TMBod and MEBod chromophores are recognizable in the window from 450 to 540 nm, while the pyrene absorption transitions dominate the near-UV region. Excitation into the PY chromophore at 365 nm leads to fluorescence from all three Bodipy-based emitters. Most of the observed fluorescence is associated with the EXBod unit, which appears at 675 nm, but this is complemented by weaker fluorescence from both MEBod and TMBod. Selective excitation into the EXBod chromophore at 595 nm gives the anticipated emission spectral profile and allows determination of Φ_F and τ_S as being 0.92 ± 0.04 and 6.0 ± 0.1 ns, respectively. Following excitation of PMEX at 310 or 505 nm, τ_S for the terminal acceptor EXBod is 6.1 ± 0.1 ns.

Fluorescence spectra recorded for MEBod and TMBod are well resolved from those recorded for EXBod (Figure S5). Following excitation of PMEX in CH_2Cl_2 at 370 nm, it was not possible to resolve emission from PY, and we assume that rapid EET occurs to one of the appended TMB units. Using time-correlated, single photon counting methodology with excitation at 340 nm, it was possible to detect fluorescence from TMB at 520 nm. The assertion of efficient EET from PY to TMB was fully supported by excitation spectra (Figure S9). Emission from TMB was found to decay with an average lifetime of 33 ± 7 ps, although this is close to the temporal resolution of our setup following numerical reconvolution of the data and the quality of the fit was quite poor.[60] There was also a minor (i.e., 8%) contribution from a longer-lived component having a lifetime of ca. 190 ps (Figure 8). Fluorescence associated with MEBod grows-in after the excitation pulse with a time constant of 30 ± 5 ps before decaying via exponential kinetics. Indeed,

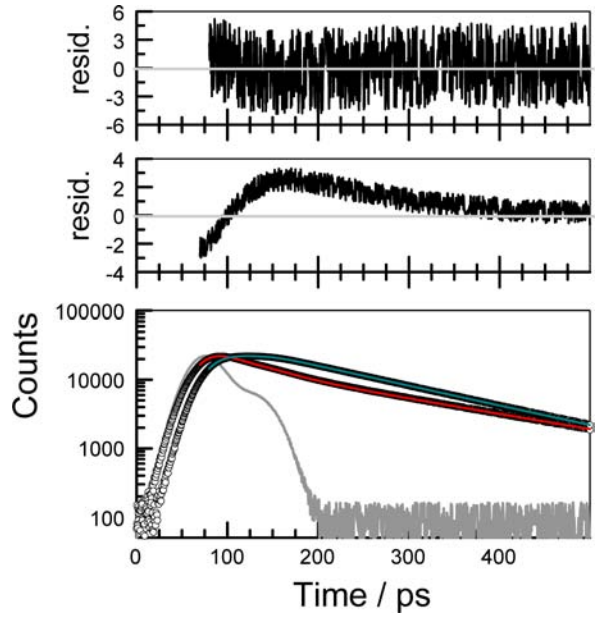

Figure 8. Time-resolved fluorescence decay profiles recorded for PMEX in CH_2Cl_2 at room temperature following excitation at 340 nm. The IRF is shown as a gray curve, while data points are shown as open circles. Nonlinear least-squares fits to the growth and decay are shown as red (TMBod at 515 nm) and blue (MEBod at 590 nm) lines superimposed on the experimental data. For MEBod, analysis corresponds to a growth of 30 ps and a decay of 148 ps, the weighted residuals (χ^2 = 1.32) being given in the upper panel. For TMBod, analysis corresponds to a dual-exponential decay of 30 ps (92%) and 190 ps (8%), with the weighted residuals (χ^2 = 1.51) being shown on the central panel.

dx.doi.org/10.1021/ja4049306 | J. Am. Chem. Soc. 2013, 135, 11330−11344

the fluorescence signal at 555 nm decayed with an average lifetime of 148 ± 9 ps (Figure 8).

Using time-correlated, single photon counting with detection across the 680−720 nm window, fluorescence associated with the EXBod acceptor grows-in after the excitation pulse (Figure 9); in contrast, direct excitation into EXBod at 635 nm gives a

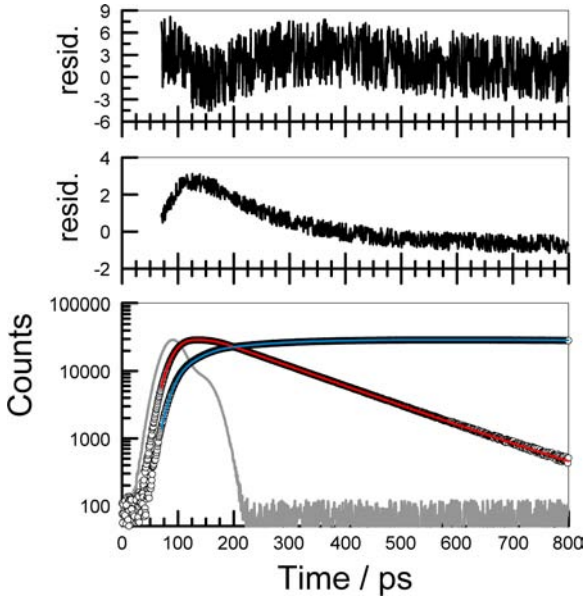

Figure 9. Time-resolved fluorescence decay profiles recorded for PMEX in CH_2Cl_2 at room temperature following excitation at 370 nm. The IRF is shown as a gray curve while data points are shown as open circles. Nonlinear least-squares fits to the growth and decay are shown as red (MEBod at 590 nm) and blue (EXBod at 720 nm) lines superimposed on the experimental data. For MEBod, analysis corresponds to a growth of 34 ps and a decay of 160 ps, the weighted residuals (χ^2 = 1.39) being given in the upper panel. For EXBod, analysis corresponds to a dual-exponential decay of 6 ns and a growth of 175 ps, with the weighted residuals (χ^2 = 1.75) being shown on the central panel.

comparable decay time of 6 ns but without the slow growth (Figure S10). The grow-in for EXBod emission following excitation at 340 nm corresponds to an average time constant of 150 ± 15 ps, followed by decay with a lifetime of 6.0 ± 0.2 ns, although it has to be stressed that the initial part of the fit is quite poor. We attribute this slow appearance of acceptor fluorescence to intramolecular EET from MEBod, in agreement with the excitation spectra (Figure S9).[61] Because of the significantly red-shifted absorption transition of the expanded Bodipy residue, spectral overlap between emission from MEBod and absorption by EXBod is kept modest[56] (J_{DA} = 0.061 cm), and this serves to restrict k_{EET}. The distance between the centers of the two reactants is ca. 21.2 Å, and on the basis of previous findings with related dyads,[27] it is likely that the dominant EET mechanism involves through-bond interactions. The spectroscopic energy gap between excited-singlet states resident on the reactants (ΔE_{SS} = 3650 cm^{-1}) is sufficient for ETT to be unidirectional. The poor fit for the appearance of EXBod emission is attributed to secondary EET events that follow from distribution of the exciton around the array. Indeed, the best analytical fit to the data after deconvolution corresponds to a decay of 6 ns but with two growth signals of 140 ps (91%) and 700 ps (9%), respectively.

Interestingly, the fluorescence spectrum shows residual emission from TMBod, although the yield is rather small (Figure 7). This finding is indicative of the thermal equilibrium between excited states resident on TMBod and MEBod being set up across the full array (consult Figure S11 for a distribution profile based on computer modeling). This situation is further testament to the relatively slow rate of EET from MEBod to EXBod in this system. Also contingent on this slow EET to the terminal acceptor is the possibility for through-space EET between the appended MEBod units, and using the same approach as illustrated for PMEt, the rate constant for this step[62] was estimated to be 1.5 × 10^8 s^{-1}. Although inefficient, this process helps to distribute the photon density around the molecular array, as illustrated in Figure S12.

The average lifetime derived for the S_1 state of MEBod in the fully array PMEX is 155 ± 20 ps, compared to the inherent lifetime of 4.6 ± 0.1 ns in CH_2Cl_2. In addition to radiative (k_{RAD} = 1.6 × 10^8 s^{-1}) and nonradiative (k_{NR} = 5.4 × 10^7 s^{-1}) decay to the ground state, deactivation of this excited state can be partitioned into contributions due to energy migration to an ancillary MEBod unit (k = 1.5 × 10^8 s^{-1}, 2%), reverse EET to one of the attached TMBod units (k = 1.0 × 10^9 s^{-1}, 15%) and EET to the terminal EXBod unit (k = 5.4 × 10^9 s^{-1}, 83%). Photons directed away from the terminal acceptor will arrive at EXBod after a short delay, and it is this branching process that accounts for the poor fit for the growth process. In fact, the best fit gives two growth steps with lifetimes of 160 ps (91%) and 700 ps (9%).

With minor modification of these EET rate constants, the steady-state emission spectrum can be recovered by computer simulation[63] assuming a static geometry and allowing for monophotonic excitation of the array (Figure S12). With this increased confidence, we can summarize the experimental results in the form of Scheme 2. Here, photons enter the array by way of PY, TMB, MEBod, or EXBod. We consider EET from PY to TMB to be both unidirectional and quantitative, while that from TMB to MEBod is too fast for significant sideways transfer to a second TMB unit. Because onward EET

Scheme 2. Pictorial Representation of EET Flow in the PMEX Array, Allowing for Excitation into Any of the Main Chromophores

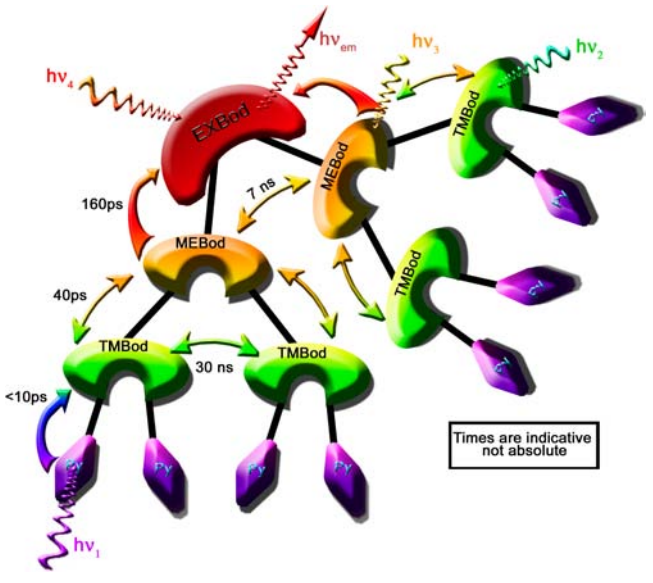

dx.doi.org/10.1021/ja4049306 | J. Am. Chem. Soc. 2013, 135, 11330−11344

from MEBod to EXBod is relatively slow, reverse EET can occur to repopulate the S_1 state of TMB. Since the system has no memory, this process will activate either of the two available TMB units. Backward EET sets up the equilibrium between S_1 states on these three chromophores such that the exciton samples all three within its lifetime of 4 ns. There is now the possibility that the exciton migrates across to the MEBod unit on the opposite branch and from there to one of the appended TMB units. This leads to widespread distribution of the exciton and causes further delay in its (almost) inevitable arrival at EXBod.

Preliminary Sensitization Studies Made with PMEX. There has been considerable interest[64,65] of late in the development of artificial light-harvesting arrays formed by mixtures of organic dyes as potential sensitizers for solar cells. We,[27] and others,[66] have shown that Bodipy dyes can be used for such purposes, while related Bodipy-based dyes have shown exceptional promise in organic devices for solar-to-electricity conversion.[67] Cascade-type arrays, such as PMEX, collect around 30% of the solar spectrum (Figure 10) and emit in the

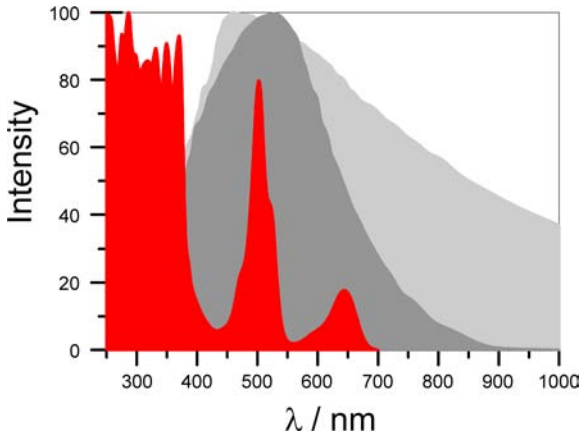

Figure 10. Crude comparison of the average solar output at AM1 (light gray curve) with the action spectrum recorded for the amorphous Si solar cell (dark gray curve) and the absorption spectrum of PMEX recorded in solution (red curve).

region where amorphous silicon and GaInP exhibit absorption thresholds. The most attractive feature of PMEX relative to a cocktail of unattached dyes is that it does not suffer from problems of self-absorption, this being the limiting factor for most organic dyes used as solar concentrators in plastic films.[68] In the solid state, it was also found that PMEX does not undergo self-quenching, again this is a major problem for simple organic dyes, probably because of its complex 3D topology.

The following experiments were made in order to demonstrate the ability of PMEX to sensitize current generation from amorphous silicon. The compound (1 mg/25 mg, w/w) was dispersed in molten sucrose octa-acetate (SOA) and used to construct a disk (1 cm diameter and 4 mm thickness). The disk was adhered to a dichroic mirror, via a thin layer of poly(methylmethacrylate), that reflects $\lambda > 650$ nm and the edges coated with reflective paint. The disk was mounted at the focal plane of a small integrating sphere and illuminated via an optical fiber with panchromatic light ($\lambda < 650$ nm). Fluorescence from the disk, isolated with a 650 nm cutoff filter, was directed through a second optical fiber and beam expander to an amorphous Si solar cell (10 × 10 mm). The excitation light was modulated at 1 kHz and the photocurrent detected at the same frequency with a lock-in amplifier. The light intensity was adjusted to give a steady output of 150 lx, resulting in an average current of 5.7 μA. Comparison was made with a conventional LED emitting at 660 ± 25 nm and collimated with an identical beam expander. Restricting light output to equal that from the SOA disk at 150 lx illumination gave a similar average photocurrent of 5.3 μA. This experiment serves to demonstrate the basic principle of sensitization.

During 100 h of continuous illumination with the LED, the current decreased by 11% and was not recovered by a dark period. The same experiment made with an SOA disk impregnated with PMEX gave a current loss of 24% over 100 h. A similar experiment made with EXBod only incorporated into the SOA disk stopped producing current after 36 h continuous illumination. Increasing the light intensity by a factor of 4-fold, achieved by removal of a neutral density filter, caused complete bleaching of EXBod in less than 24 h illumination. The high photon flux was much less harmful to the PMEX disk, although the photocurrent dropped by almost 35% during 100 h illumination. This can be compared with a current loss of 18% with the LED. Interestingly, the initial current increased a factor of almost 4-fold for the LED at the higher photon flux, but the increase for PMEX was only from 5.7 to 14.1 μA. This might be the onset of photon management due to the anticipated photoregulation. Although far from definitive, these initial results hold promise for the design of photostable arrays. It should also be noted that PMEX has a built-in capability to dissipate UV photons via rapid internal conversion and EET. This stabilizes the dye against UV damage, which is harmful to the Si solar cell. Thus, direct illumination of the Si solar cell with UV light at $290 < \lambda < 340$ nm causes rapid loss of current but this does not occur when the SOA/PMEX disk is in place. In passing, we note that output from PMEX is of the optimum color for stimulated plant growth using far red light.[69] This might be a further application[70] for such arrays, especially if the photoregulatory effect can be perfected.

The illumination levels used for these experiments were kept quite low, and it is questionable if, under these conditions, more than one photon is present on the array at any given time. Certainly, the time between absorption of successive photons is likely to be much longer than the EET time scales.[71] As such, the improved photostability found for PMEX relative to EXBod cannot be ascribed simply to redistribution of photons around the array. To further explore this situation, the following experiment was performed: A thick (ca. 2 mm) film of PMEX in poly(methylmethacrylate) was illuminated with a train of 5 ns laser pulses at 355 nm. The laser beam was passed through a pinhole (diameter 0.25 cm) before the sample and the intensity were adjusted to be within the range 0–25 mJ per pulse at a repetition rate of 10 Hz. The fluorescence spectrum was recorded with a spectrograph over the wavelength range 500–700 nm, which allows estimation of the ratio of emission bands for EXBod and MEBod. The ratio found at low laser intensity (3 mJ per pulse), adjusted with metal screen filters, was roughly in agreement with that seen from steady-state emission spectra, but it did not change significantly with increasing laser power. Under these conditions, the time between incoming photons is very long relative to the EET events, and on simple statistical grounds, the likelihood of a single molecule of PMEX absorbing two photons is <20%. Since higher photon densities are

attainable with shorter pulse durations, attention was turned toward transient absorption spectroscopy.

Transient Absorption Spectroscopy with PMEt. The transient differential absorption spectrum recorded for **4** in MTHF following excitation at 420 nm with a 20 ps laser pulse is shown in Figure S13. The negative signal observed across the region from 500 to 570 nm corresponds to a combination of ground-state bleaching and stimulated fluorescence. These contributions are superimposed onto a broad, relatively weak absorption band that must correspond to the S_1-S_n transition. The latter appears on either side of the bleaching signal. By subtracting combined spectra for the emission and ground-state bleach, using an iterative routine to optimize the band shape,[72] the actual absorption spectrum for the Bodipy-based excited-singlet state can be revealed (Figure S13). This latter band is diffuse but centered at ca. 480 nm. It overlaps with fluorescence from the TMBod chromophore, although the optical absorption transition is quite weak relative to bleaching of the ground state so the molar absorption coefficient must be small throughout the overlap region. Under these conditions, the signal decays with a lifetime in the ns range and is formed within the excitation pulse. Experiments carried out with TMBod show remarkably similar behavior.

Using the above results to assist interpretation, transient absorption spectral studies were made with PMEt in MTHF following laser excitation into the PY chromophore at 355 nm with a 9 ps laser pulse (Figure 11). The pulse width is

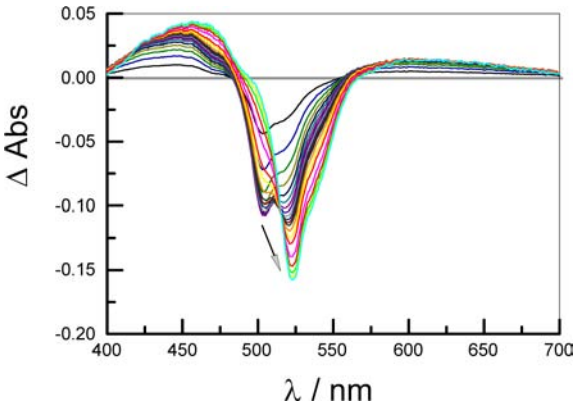

Figure 11. Transient differential absorption spectra recorded after laser excitation of PMEt in MTHF at 355 nm. Spectra were recorded across the time window between 0 and 200 ps, with the arrow indicating the course of the spectral changes.

comparable to the EET time scale and longer than vibrational relaxation,[49] but nonetheless the transient spectral records can be used to confirm EET from TMBod to MEBod. The rate constant for the latter process, as derived by global analysis[72] across the wavelength range from 500 to 540 nm, is 2.7×10^{10} s^{-1} and remains in reasonable agreement with the time-resolved emission data. The main spectral changes observed at low laser intensity concern a gradual shift of the bleaching maximum from ca. 500 to ca. 520 nm as EET proceeds. The final signal hardly decays over a few hundred ps or so and corresponds to the thermally established equilibrium of singlet-excited states associated with the two Bodipy-based chromophores; clearly the final signal is dominated by the exciton localized on MEBod. Representative kinetic traces are shown in Figure 12 and confirm the EET pathway derived from the emission studies.

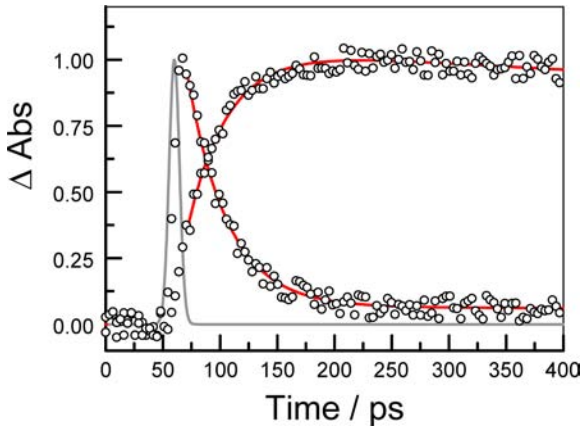

Figure 12. Representative kinetic traces recorded for bleaching of TMBod at 500 nm and MEBod at 535 nm following excitation of PMEt at 355 nm with a low intensity pulse. The Gaussian IRF inferred from autocorrelation of the 1064 nm pulse is shown as a gray curve. Experimental data are shown as open circles, and the fit to the data is given as a red line. Data points are normalized at the peak channel and inverted for easier presentation.

For the above experiment, the laser intensity was kept to a low level, being equivalent to 2×10^{16} photons/cm^2 s, so as to minimize the possibility to excite multiple PY units on a given molecule. Using a slight modification of the protocol introduced by Melnikov et al.[31b] to allow for the 3D nature of the sample, calculations for the 10 MHz repetition rate indicate that the probability of adding one, two, or three photons to PMEt is 0.16, 0.012 and 0, respectively. At the highest accessible laser intensity (i.e., 2×10^{17} photons/cm^2 s), the same probabilities are calculated to be 0.37, 0.53, and 0.05. These are the optimized conditions for attaching two photons onto the array, at least with our available equipment. As a convenient means by which to monitor the course of EET, we restrict attention to two fixed wavelengths corresponding to deactivation of the S_1 state of TMBod and appearance of the corresponding S_1 state associated with MEBod. The initial part of the bleaching signal is eliminated from the analysis on the basis that it could be contaminated with contributions from vibrational cooling and signals due to direct excitation by MEBod.

At low laser intensity, the transient absorption signal from TMBod grows in within the Gaussian-shaped pulse and decays with a time constant of 32 ps. There is a minor component amounting to ca. 8% that decays very slowly and is attributed to the equilibrium mixture of excited states. Bleaching of MEBod can be accommodated with first-order kinetics, having a lifetime of 35 ps, while decay is on the ns time scale (Figure 12). The situation at the highest laser intensity is similar, except that recovery of the TMBod signal occurs on a slower time scale, corresponding to a first-order lifetime of 46.5 ps. Again, the bleaching occurs with a time constant of 10 ps, and there is a minor contribution from a very long-lived component. At 535 nm, bleaching of the MEBod chromophore occurs with a time constant of 49.6 ps before recovery on the ns time scale (Figure 13). The quality of the experimental data, together with the complexity of the reaction scheme, precludes more protracted data analysis. In fact, we emphasize that other kinetic models, such as a stretched exponential, will also fit the data[73,74] One possible explanation for this lengthening of the mean lifetime involves relatively slow S_1-S_1 annihilation between excitons

dx.doi.org/10.1021/ja4049306 | J. Am. Chem. Soc. 2013, 135, 11330−11344

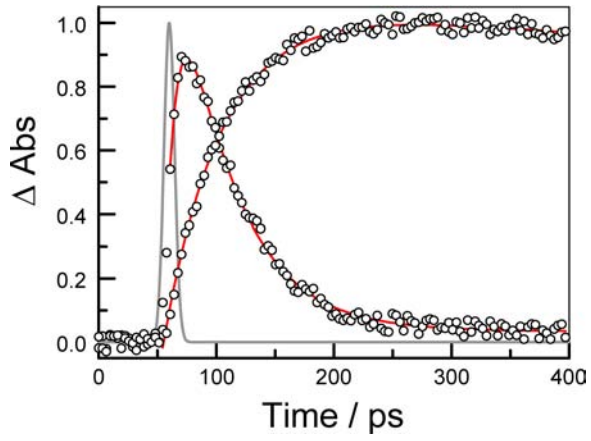

Figure 13. Representative kinetic traces recorded for bleaching of TMBod at 500 nm and MEBod at 535 nm following excitation of PMEt at 355 nm with a high intensity pulse. The Gaussian IRF inferred from autocorrelation of the 1064 nm pulse is shown as a gray curve. Experimental data are shown as open circles, and the fit to the data is given as a red line. Data points are normalized at the peak channel and inverted for easier presentation.

localized on MEBod and TMBod (Scheme 3). We presume that the resultant doubly excited state of whichever

Scheme 3. Illustration of the Delayed EET Step Expected for PMEt at High Excitation Densities

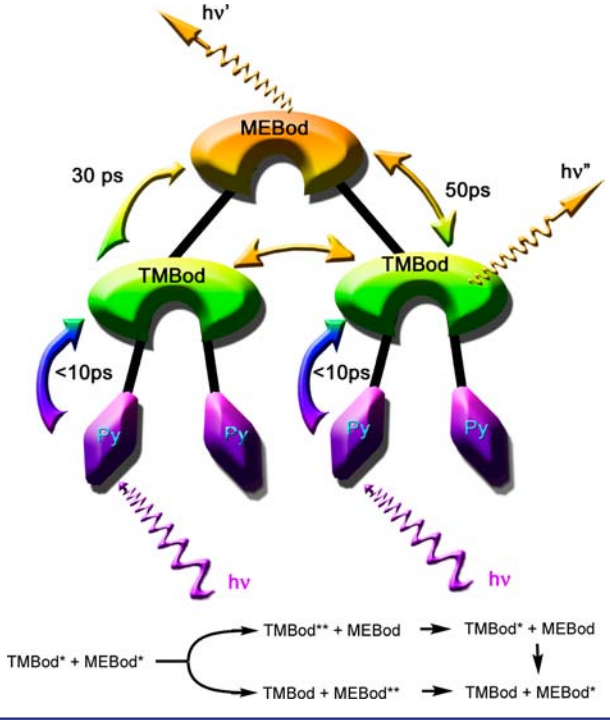

chromophore undergoes rapid internal relaxation to form the S_1 state, with subsequent loss of the excess photonic energy as heat.

Two obvious possibilities coexist to explain this situation: The first case requires slow EET from TMBod* to MEBod*, which could be explained in terms of the smaller spectral overlap integral (J_{DA}). Thus, for EET from the first-excited singlet state (S_1) of TMBod to the ground state (S_0) of MEBod, J_{DA} is calculated[56] from the respective emission and absorption spectra to be 0.59 cm. For the corresponding EET step from TMBod* to MEBod*, J_{DA} is calculated to be 0.19 cm. The rate of ETT is expected[75] to vary in a linear manner with J_{DA} unless other factors, notably the coupling matrix element, change significantly. A case could be made, therefore, for this type of exciton blockade. In fact, the relevant energy gaps also change for the two processes; the energies of the S_1 states localized on donor and acceptor, taken as the overlap between normalized absorption and emission spectra, are 19 630 and 18 840 cm^{-1}, respectively, for TMBod and MEBod, while the S_2 state associated with MEBod lies at 24 390 cm^{-1}. As such, there is little excess energy (i.e., 790 cm^{-1}) to be dissipated during EET to the ground state but EET to the upper-lying S_2 state requires loss of some 17 870 cm^{-1} by way of vibrational cooling. This will likely contribute toward a decreased rate of through-bond EET to the S_2 state.[76]

The second case involves (reverse) EET from MEBod* to TMBod*, such that the surviving exciton is associated with the higher-energy S_1 localized on TMBod. This situation is in accord with the energy-gap law[77] but still demands dissipation of excess energy as heat. The consequence of such annihilation is that the surviving exciton will be transferred to the MEBod acceptor. There will be a delay in the average arrival time corresponding to the mean time taken for the annihilation step. In the absence of further information, it is assumed that S_1-S_1 annihilation shows little preference for which chromophore retains the exciton.

In other systems where an exciton blockade has been considered,[28] it has been necessary to draw attention to alternative possibilities, such as bleaching of the acceptor,[78] conformational exchange,[31] or triplet formation.[79] In the case of PMEt, a potential escape path for the exciton involves interbranch energy migration between TMBod units. This route was ignored earlier on the basis that the average center-to-center separation distance of 29 Å is too long for competing EET given the relative efficacy of onward EET to MEBod. However, certain molecular conformations will be especially favorable for fast EET between TMBod molecules since their transition dipole moment vectors are perfectly aligned for through-space interactions. It is also recognized[80] that Förster theory tends to underestimate the rate of EET at short separations; the closest edge-to-edge approach between the two reactants is ca. 18 Å. In the extreme case, interbranch EET within this family of conformers could reach 5×10^8 s^{-1}. The net result is that any factor that slows the rate of onward EET could promote sideways EET between TMBod sites. This, in turn, would delay arrival of the second photon at the acceptor.

Transient Absorption Spectroscopy with PMEX. Singlet–singlet exciton annihilation is well-known in dendrimers,[81] conducting polymers,[82] and other molecular clusters.[83] However, the behavior recorded for PMEt is unusual in that the rate of annihilation appears to be slow relative to EET to the ground-state acceptor; it has to be recognized that, in many clusters, the rate of annihilation reflects the molecular topology such that comparisons between different systems is not straightforward. Although the time constants for successive EET at high photon flux cannot be vastly different, the molecule could be deemed to possess the capacity to "hold" the extra photon. It is interesting to note in this context that there have been several attempts to develop protocols for mapping excitonic flow in complex molecular architectures.[84] Extending the work to include EXBod is made difficult by the realization that the excitation conditions for attaching only two photons

dx.doi.org/10.1021/ja4049306 | J. Am. Chem. Soc. 2013, 135, 11330–11344

onto the array cannot be identified. The best conditions, at least according to our models,[31b] allow for a probability distribution of the type 0.32, 0.38, 0.20, and 0.02, respectively, for adding one, two, three or four photons to the network.

Working within this constraint, laser flash photolysis studies were made for PMEX in CH_2Cl_2 with excitation at 355 nm and using the conditions optimized to give the above excitation density (Figure S14). First, experiments were made at an excitation intensity 10-fold lower than the optimum value; this is intended to serve as a low-intensity control. These conditions give a projected probability distribution that favors mono-excitation (i.e., 0.16, 0.013, and 0 for addition of 1, 2, and 3 photons to the cluster). Bleaching of the EXBod chromophore follows first-order kinetics with an average lifetime of 153 ± 8 ps. Again, the initial part of the bleaching curve was omitted from the analysis. Recovery of the ground-state signal at 647 nm also follows first-order kinetics and corresponds to a lifetime of ca. 2.8 ± 0.3 ns. The data relating to bleaching and recovery of TMBod are very noisy but give a crude estimate of the lifetime for the recovery step as being 30 ± 8 ps. Meanwhile, bleaching and recovery of MEBod gives analyzed lifetimes of 26 ± 4 and 139 ± 9 ps, respectively (Figure 14). These values seem to be in surprisingly good accord with data obtained by time-resolved emission spectroscopy, although the latter are believed to be far more precise.

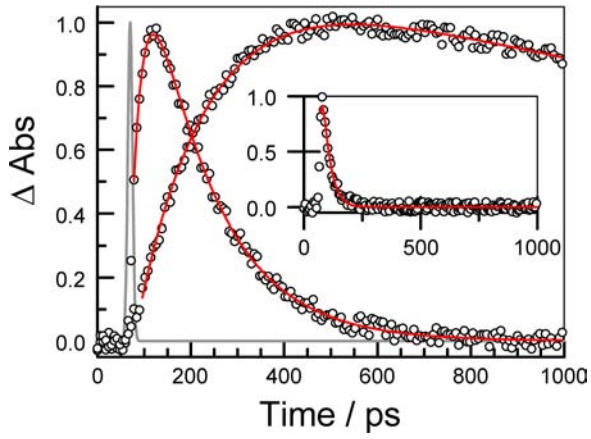

Figure 14. Representative kinetic traces recorded for bleaching of EXBod at 647 nm and MEBod at 535 nm following excitation of PMEX at 355 nm with a low intensity pulse. The Gaussian IRF inferred from autocorrelation of the 1064 nm pulse is shown as a gray curve. Experimental data are shown as open circles, and the fit to the data is given as a red line. Data points are normalized at the peak channel and inverted for easier presentation. The insert shows the corresponding data for TMBod.

Interrogation of the system at the higher laser power shows that, in this case, transient bleaching of EXBod occurs on a slightly slower time scale. Thus, the time constant for transient bleaching of the terminal acceptor is lengthened to ca. 170 ± 8 ps, while that for recovery remains at 2.8 ± 0.3 ns. In addition, the recovery of MEBod bleaching is somewhat slower than found at low-light intensity, the time constant increasing from 139 to 150 ps. Thus, kinetic indicators for some type of exciton blockage, or energy pooling,[71] are less evident for the full array. This might be expected from the respective spectral overlap integrals; J_{DA} for conventional (i.e., MEBod* to EXBod) EET being 0.061 cm, while that for the second step (i.e., MEBod* to EXBod*) is 0.225 cm. The resultant doubly excited state of EXBod (i.e., EXBod**) is expected to decay rapidly to form the corresponding S_1 state. Backward EET (from EXBod* to MEBod* to give MEBod**) should be promoted by the energy-gap law[77] and by the modest spectral overlap integral (J_{DA} = 0.0052 cm) to such an extent that it might be competitive with forward annihilation. As such, this remains the most likely route for the observed retardation of the bleaching kinetics. There is no obvious indication for charge transfer between the two dyes, as happens in certain singlet−singlet annihilation processes, but this cannot be ruled out entirely.

■ CONCLUDING REMARKS

The molecular topology inherent to PMEX funnels photons absorbed by the various subunits to the terminal acceptor with small losses at each stage. It is also interesting to note the stepwise fall in the rate of EET on moving along the energy gradient. Reversible EET and through-space couplings allow exciton distribution over much of the array at low photon flux. This behavior is not unique, and sequential EET has been widely reported in dendrimers[37] and conducting polymers.[38] In part, this situation arises from the logical positioning of chromophores in PMEX that directs photons along convergent pathways. Although unusual, we have to question the advantage offered by such photon redistribution in terms of either efficiency or self-protection of the array. At low-light levels under conditions where there is fast discharge of photons from EXBod to a solar cell, the distributive mechanism is redundant, and the limiting step is EET from MEBod to EXBod. On average, an absorbed photon reaches the terminal acceptor within a few hundred picoseconds, and overall EET to the terminal should exceed 90% despite the slow rate for the final step. Increasing the fraction of sunlight harvested by the array and optimizing the threshold wavelength for the terminal acceptor are well within the synthetic capability. Thus, within this constraint, PMEX serves as a useful artificial leaf. Future development of this type of system will involve accreting numerous such units[39] into a cooperative network where EET can occur between PMEX units. In this respect, the use of supramolecular interactions[40] is considered mandatory.

At high-photon densities, PMEX possesses three separate junctions where photon annihilation might take place. Although such reactions lose excitation energy as low-grade heat, there is little propensity for triplet formation,[25a] and the molecule is quite stable toward photodegradation when dispersed in SOA, especially under UV illumination. A crude estimate for the photon turnover frequency is ca. 0.1 Hz such that each chromophore has an average turnover number in excess of 10 000 during sensitization. As such, it appears that the system provides a relatively effective means for photon management. As the rate of discharge becomes slower, or in cases where the light intensity fluctuates, there could be escalating significance for a redistributive system. Clearly, the kinetic balance becomes critical, and the overall system seems to be an ideal vehicle for sophisticated molecular simulations.[84] On-going research aims to increase Φ_F for the terminal acceptor and to add additional relays.

■ ASSOCIATED CONTENT

Supporting Information

Full synthetic details, experimental methods, additional examples of experimental output, and examples of NMR spectra. This material is available free of charge via the Internet at http://pubs.acs.org.

dx.doi.org/10.1021/ja4049306 | J. Am. Chem. Soc. 2013, 135, 11330−11344

AUTHOR INFORMATION

Corresponding Author

Anthony.harriman@ncl.ac.uk; ziessel@unistra.fr

Notes

The authors declare no competing financial interest.

ACKNOWLEDGMENTS

We thank CNRS, EPSRC, and Newcastle University for financial support of this work.

REFERENCES

(1) (a) Lewis, N. S. *Nature* **2001**, *414*, 589−590. (b) Blankenship, R. E. *Molecular Mechanisms of Photosynthesis*; Blackwell Science: Oxford, 2002. (c) Zhu, X.-G.; Long, S. P.; Ort, D. R. *Ann. Rev. Plant Biol.* **2010**, *61*, 235−261. (d) Ziessel, R.; Harriman, A. *Chem. Commun.* **2011**, *47*, 611−631.

(2) Quina, F. H.; Moreira, P. F.; Vautier-Giongo, C., Jr.; Rettori, D.; Rodrigues, R. F.; Freitas, A. A.; Silva, P. F.; Maçanita, A. L. *Pure Appl. Chem.* **2009**, *81*, 1687−1694 and references cited therein.

(3) (a) Holten, D.; Bocian, D. F.; Lindsey, J. S. *Acc. Chem. Res.* **2002**, *35*, 57−69. (b) Harriman, A.; Ziessel, R. In *Carbon-Rich Compounds*; Haley, M. M., Tykwinski, R. R., Eds.; Wiley-VCH: Weinheim, 2006; pp 26−89.

(4) (a) Nakamura, Y.; Aratani, N.; Osuka, A. *Chem. Soc. Rev.* **2007**, *36*, 831−845. (b) Armaroli, N.; Balzani, V. *Angew. Chem., Int. Ed.* **2007**, *46*, 52−66.

(5) (a) Serin, J. M.; Brousmiche, D. W.; Fréchet, J. M. J. *Chem. Commun.* **2002**, 2605−2607. (b) Weil, T.; Reuther, E.; Müllen, K. *Angew. Chem., Int. Ed.* **2002**, *41*, 1900−1904.

(6) (a) Earp, A. A.; Smith, G. B.; Franklin, J.; Swift, P. *Sol. Energy Mater. Sol. Cells* **2004**, *84*, 411−421. (b) Brühwiler, D.; Calzaferri, G.; Torres, T.; Ramm, J. H.; Gartmann, N.; Dieu, L.-Q.; Lopez-Duarte, I.; Martinez-Diaz, M. V. *J. Mater. Chem.* **2009**, *19*, 8040−8067. (c) Knuesel, R. J.; Jacobs, H. O. *Adv. Mater.* **2011**, *23*, 2727−2733.

(7) (a) Dienel, T.; Bauer, C.; Dolamic, I.; Brühwiler, D. *Solar Energy* **2010**, *84*, 1366−1369. (b) Ziessel, R.; Goze, C.; Ulrich, G.; Cesario, M.; Retailleau, P.; Harriman, A.; Rostron, J. P. *Chem.—Eur. J.* **2005**, *11*, 7366−7378.

(8) (a) Silva, P. F.; Paulo, L.; Barbafina, A.; Eisei, F.; Quina, F. H.; Maçanita, A. L. *Chem.—Eur. J.* **2012**, *18*, 3736−3744. (b) Bora, D. K.; Rozhkova, E. A.; Schrantz, K.; Wyss, P. P.; Braun, A.; Graule, T.; Constable, E. C. *Adv. Funct. Mater.* **2012**, *22*, 490−502.

(9) Ahn, T. K.; Avenson, T. J.; Ballottari, M.; Cheng, Y.-C.; Niyogi, K. K.; Bassi, R.; Fleming, G. R. *Science* **2008**, *320*, 794−797.

(10) (a) Purcell, E. B.; Crosson, S. *Curr. Opin. Microbiol.* **2008**, *11*, 168−178. (b) Matsuoka, D.; Iwata, T.; Zikihara, K.; Kandori, H.; Tokutomi, S. *Photochem. Photobiol.* **2007**, *83*, 122−130. (c) Gust, D.; Moore, T. A.; Moore, A. L. *Faraday Discuss.* **2012**, *155*, 9−26.

(11) Boghossian, A. A.; Ham, M.-H.; Choic, J. H.; Strano, M. S. *Energy Environ. Sci.* **2011**, *4*, 3834−3843.

(12) Wagner, S.; Bauer, S. *MRS Bull.* **2012**, *37*, 207−217 and refs therein.

(13) (a) Zhang, J.; Hoeben, F. J. M.; Pouderoijen, M. J.; Schenning, A. P. H. J.; Meijer, E. W.; De Schryver, F. C.; De Feyter, S. *Chem.—Eur. J.* **2006**, *12*, 9046−9055. (b) Werwie, M.; Xu, X. X.; Haase, M.; Basche, T.; Paulsen, H. *Langmuir* **2012**, *28*, 5810−5818.

(14) (a) Loudet, A.; Burgess, K. *Chem. Rev.* **2007**, *107*, 4891−4932. (b) Ulrich, G.; Ziessel, R.; Harriman, A. *Angew. Chem., Int. Ed.* **2008**, *47*, 1184−1201.

(15) (a) Ziessel, R.; Ulrich, G.; Harriman, A. *New J. Chem.* **2007**, *31*, 496−501. (b) Ziessel, R. *C. R. Chim.* **2007**, *10*, 622−629.

(16) Boens, N.; Leen, V.; Dehaen, W. *Chem. Soc. Rev.* **2012**, *41*, 1130−1172.

(17) (a) Bozdemir, O. A.; Erbas-Cakmak, S.; Ekiz, O. O.; Dana, A.; Akkaya, E. U. *Angew. Chem., Int. Ed.* **2011**, *50*, 10907−10912. (b) Haefele, A.; Ulrich, G.; Retailleau, P.; Ziessel, R. *Tetrahedron Lett.* **2008**, *49*, 3716−3721. (c) Ziessel, R.; Goze, C.; Ulrich, G. *Synthesis* **2007**, 936−949. (d) Nastasi, F.; Puntoriero, F.; Campagna, S.; Olivier, J.-H.; Ziessel, R.. *Phys. Chem. Chem. Phys.* **2010**, *12*, 7392−7402. (e) Goeb, S.; Ziessel, R. *Tetrahedron Lett.* **2008**, *49*, 2569−2574. (f) Goze, C.; Ulrich, G.; Mallon, L. J.; Allen, B. D.; Harriman, A.; Ziessel, R. *J. Am. Chem. Soc.* **2006**, *128*, 10231−10239.

(18) Hara, T.; Hirasawa, A.; Sun, Q.; Koshimizu, T.-A.; Itsubo, C.; Sadakane, K.; Awaji, T.; Tsujimoto, G. *Mol. Pharmacol.* **2009**, *75*, 85−91.

(19) Ulrich, G.; Goze, C.; Guardigli, M.; Roda, A.; Ziessel, R. *Angew. Chem., Int. Ed.* **2005**, *44*, 3694−3698.

(20) Zheng, Q.; Xu, G.; Prasad, P. N. *Chem.—Eur. J.* **2008**, *14*, 5812−5819.

(21) Niu, S. L.; Massif, C.; Ulrich, G.; Ziessel, R.; Renard, P.-Y.; Romieu, A. *Org. Biomol. Chem.* **2011**, *9*, 66−69.

(22) (a) Johnson, I., Spence, M., Eds.*The Molecular Probes Handbook. A Guide to Fluorescent Probes and Labelling Technologies*, 11th ed.; Life Technologies: Eugene, OR, 2010. (b) Bricks, J. L.; Kovalchuk, A.; Trieflinger, C.; Nofz, M.; Büschel, M.; Tolmachev, A. I.; Daub, J.; Rurack, K. *J. Am. Chem. Soc.* **2005**, *127*, 13522−13529.

(23) Didier, P.; Ulrich, G.; Mély, Y.; Ziessel, R. *Org. Biomol. Chem.* **2009**, *7*, 3639−3642.

(24) (a) Barin, G.; Yilmaz, M. D.; Akkaya, E. U. *Tetrahedron Lett.* **2009**, *50*, 1738−1740. (b) Liu, J. Y.; Ermilov, E. A.; Roder, B.; Ng, D. K. P. *Chem. Commun.* **2009**, 1517−1519. (c) Camerel, F.; Ulrich, G.; Retailleau, P.; Ziessel, R. *Angew. Chem., Int. Ed.* **2008**, *46*, 8876−8880. (d) Zhang, X. L.; Xiao, Y.; Qian, X. H. *Org. Lett.* **2008**, *10*, 29−32. (e) Isaksson, M.; Hagglof, P.; Hakansson, P.; Ny, T.; Johansson, L. B. Å. *Phys. Chem. Chem. Phys.* **2007**, *9*, 3914−3922. (f) Coskun, A.; Akkaya, E. U. *J. Am. Chem. Soc.* **2006**, *128*, 14474−14475. (g) Yilmaz, M. D.; Bozdemir, O. A.; Akkaya, E. U. *Org. Lett.* **2006**, *8*, 2871−2873. (h) Kalinin, S.; Johansson, L. B. Å. *J. Phys. Chem. B* **2004**, *108*, 3092−9097. (i) Keller, R. C. A.; Silvius, J. R.; de Kruijff, B. *Biochem. Biophys. Res. Commun.* **1995**, *207*, 508−514.

(25) (a) Harriman, A.; Mallon, L. J.; Ziessel, R. *Chem.—Eur. J.* **2008**, *14*, 11461−11473. (b) Harriman, A.; Mallon, L. J.; Goeb, S.; Ziessel, R. *Phys. Chem. Chem. Phys.* **2007**, *9*, 5199−5201. (c) Harriman, A.; Mallon, L. J.; Goeb, S.; Ulrich, G.; Ziessel, R. *Chem.—Eur. J.* **2009**, *15*, 4553−4560.

(26) Goze, C.; Ulrich, G.; Ziessel, R. *J. Org. Chem.* **2007**, *72*, 313−322.

(27) Harriman, A.; Mallon, L. J.; Elliot, K. J.; Haefele, A.; Ulrich, G.; Ziessel, R. *J. Am. Chem. Soc.* **2009**, *131*, 13375−13386.

(28) Berglund, A. J.; Doherty, A. C.; Mabuchi, H. *Phys. Rev. Lett.* **2002**, *89*, 068101.

(29) Birnbaum, K. M.; Boca, A.; Miller, R.; Boozer, A. D.; Northup, T. E.; Kimble, H. J. *Nature* **2005**, *436*, 87−90.

(30) (a) Nirmal, M.; Babbousi, B. O.; Bawendi, M. G.; Macklin, J. J.; Trautman, J. K.; Harris, T. D.; Brus, L. E. *Nature* **1996**, *387*, 802−804. (b) Jordens, S.; De Belder, G.; Lor, M.; Schweitzer, G.; Van der Auweraer, M.; Weil, T.; Reuther, E.; Müllen, K.; De Schryver, F. C. *Photochem. Photobiol. Sci.* **2003**, *2*, 177−186. (c) Neuwahl, F. V. R.; Righini, R.; Adronov, A.; Malenfant, P. R. L.; Fréchet, J. M. J. *J. Phys. Chem. B* **2001**, *105*, 1307−1312.

(31) (a) Cotlet, M.; Gronheid, R.; Habuchi, S.; Stefan, A.; Barbafina, A.; Müllen, K.; Hofkens, J.; De Schryver, F. C. *J. Am. Chem. Soc.* **2003**, *125*, 13609−13617. (b) Melnikov, S. M.; Yeow, E. K. L.; Uji-i, H.; Cotlet, M.; Müllen, K.; De Schryver, F. C.; Enderlein, J.; Hofkens, J. *J. Phys. Chem. B* **2007**, *111*, 708−719.

(32) (a) Wozniak, A. K.; Schroeder, G. F.; Grubmueller, H.; Seidel, C. A. M.; Oesterheit, F. *Proc. Natl. Acad. Sci. U.S.A.* **2008**, *105*, 18337−18342. (b) Alamiry, M. A. H.; Hagan, J. P.; Harriman, A.; Bura, T.; Ziessel, R. *Chem. Sci.* **2012**, *3*, 1041−1048.

(33) Hablot, D.; Ziessel, R.; Alamiry, M. A. H.; Bahraidah, E.; Harriman, A. *Chem. Sci.* **2013**, *4*, 444−453.

(34) (a) Weil, T.; Reuther, E.; Beer, C.; Müllen, K. *Chem.—Eur. J.* **2004**, *10*, 1398−1414. (b) Schweitzer, G.; Gronheid, R.; Jordens, S.; Lor, M.; De Belder, G.; Weil, T.; Reuther, E.; Müllen, K.; De Schryver, F. C. *J. Phys. Chem. A* **2003**, *107*, 3199−3207.

(35) (a) Thomas, J. K. R.; Thompson, A. L.; Sivakumar, A. V.; Bardeen, C. J. *J. Am. Chem. Soc.* **2005**, *127*, 373−383. (b) Marchi, E.; Baroncini, M.; Bergamini, G.; Van Heyst, J.; Vögtle, F.; Ceroni, P. *J. Am. Chem. Soc.* **2012**, *134*, 15277−15280. (c) Cotlet, M.; Vosch, T.; Habuchi, S.; Weil, T.; Müllen, K.; Hofkens, J.; De Schryver, F. C. *J. Am. Chem. Soc.* **2005**, *127*, 9760−9768. (d) Augulis, R.; Pugzlys, A.; Hurenkamp, J. H.; Feringa, B. L.; van Esch, J. H.; Loosdrecht, P. H. M. *J. Phys. Chem. A* **2007**, *111*, 12944−12953.

(36) (a) Meskers, S. C. J.; Bender, M.; Hubner, J.; Romanovskii, Y. V.; Oestreich, M.; Schenning, A. P. H. J.; Meijer, E. W.; Bassler, H. *J. Phys. Chem. A* **2001**, *105*, 10220−10229. (c) Megow, J.; Roder, B.; Kulesza, A.; Bonacic-Koutecky, V.; May, V. *ChemPhysChem* **2011**, *12*, 645−656.

(37) (a) Vosch, T.; Cotlet, M.; Hofkens, J.; Van der Biest, K.; Lor, M.; Weston, K.; Tinnefeld, P.; Sauer, M.; Latterini, L.; Müllen, K.; De Schryver, F. C. *J. Phys. Chem. A* **2003**, *107*, 6920−6931. (b) Maus, M.; Mitra, S.; Lor, M.; Hofkens, J.; Weil, T.; Herrmann, A.; Müllen, K.; De Schryver, F. C. *J. Phys. Chem. A* **2001**, *105*, 3961−3966.

(38) (a) Cornil, J.; Beljonne, D.; Calbert, J. P.; Brédas, J. L. *Adv. Mater.* **2001**, *13*, 1053−1067. (b) Schwartz, B. J. *Annu. Rev. Phys. Chem.* **2003**, *54*, 141−172. (c) Scholes, G. D.; Rumbles, G. *Nat. Mater.* **2006**, *5*, 683−696.

(39) Iehl, J.; Nierengarten, J. F.; Harriman, A.; Bura, T.; Ziessel, R. *J. Am. Chem. Soc.* **2012**, *134*, 988−998.

(40) Olivier, J. H.; Barbera, J.; Bahaidarah, E.; Harriman, A.; Ziessel, R. *J. Am. Chem. Soc.* **2012**, *134*, 6100−6103.

(41) (a) Katan, C.; Terenziani, F.; Mongin, O.; Werts, M. H. V.; Porres, L.; Pons, T.; Metz, J.; Tretiak, S.; Blanchard-Desce, M. *J. Phys. Chem. A* **2005**, *109*, 3024−3037. (b) Oliva, M. M.; Casado, J.; Hennrich, G.; Navarette, J. T. L. *J. Phys. Chem. B* **2006**, *110*, 19198−19206.

(42) Wrigge, G.; Gerhardt, I.; Hwang, J.; Zymofen, G.; Sandoghdar, V. *Nat. Phys.* **2008**, *4*, 60−66.

(43) (a) Mishra, A.; Behera, R. K.; Behera, P. K.; Mishra, B. K.; Behera, G. B. *Chem. Rev.* **2000**, *100*, 1973−2011. (b) Fabian, M.; Nakazumi, H.; Matsuka, M. *Chem. Rev.* **1992**, *92*, 1197−1226. (c) Yuan, M.; Yin, X.; Zheng, H.; Ouyang, C.; Zuo, Z.; Liu, H.; Li, Y. *Chem.—Asian J.* **2009**, *4*, 707−713.

(44) Harriman, A.; Heitz, V.; Ebersole, M.; Van Willigen, H. *J. Phys. Chem.* **1994**, *98*, 4982−4989.

(45) Haefele, A.; Ulrich, G.; Retailleau, P.; Ziessel, R. *Tetrahedron Lett.* **2008**, *49*, 2774−2782.

(46) Liu, T.; Morisaki, Y.; Cunningham, N.; Tykwinski, R. R. *J. Org. Chem.* **2007**, *72*, 9622−9629.

(47) Goze, C.; Ulrich, G.; Ziessel, R. *Org. Lett.* **2006**, *8*, 4445−4448.

(48) Harriman, A.; Izzet, G.; Ziessel, R. *J. Am. Chem. Soc.* **2006**, *128*, 10868−10875.

(49) (a) Hissler, M.; Harriman, A.; Khatyr, A.; Ziessel, R. *Chem.—Eur. J.* **1999**, *11*, 3366. (b) Although the various Bodipy-based chromophores do absorb at 365 nm, the stoichiometry and molar absorption coefficients indicate that direct excitation of these units never exceeds ca. 7%. This was confirmed using stoichiometric mixtures of the isolated reagents.

(50) Ziessel, R.; Rihn, S.; Harriman, A. *Chem.—Eur. J.* **2010**, *16*, 11942−11953.

(51) (a) Burghart, A.; Thoresen, L. H.; Che, J.; Burgess, K.; Bergström, F.; Johansson, L. B Å. *Chem. Commun.* **2000**, 2203−2202. (b) Wan, C.-W.; Burghart, A.; Chen, J.; Bergström, F.; Johansson, L. B. Å.; Wolford, M. F.; Kim, T. G.; Topp, M. R.; Hochstrasser, R. M.; Burgess, K. *Chem.—Eur. J.* **2003**, *9*, 4430−4441. (c) The connections to the various Bodipy fragments do not promote observable electronic interactions between bridge and dye. The absorption and emission spectra of the latter are not perturbed by these linkages, and so comparison can be made with the isolated reagents.

(52) Fluorescence quantum yields measured for the individual reference compounds are as follows: 1-ethynylpyrene $\Phi_F = 0.80$; **1** $\Phi_F = 0.78$; and **4** $\Phi_F = 0.75$. Experiments made with a 4:2:1 molar mixture of these three compounds in MTHF show emission only from PY under illumination at 365 nm.

(53) Because the derived lifetime is close to the limit of the temporal resolution of this setup, we should treat the absolute value with caution. The underlying trend is correct, but the magnitude of the short component might not be as stated, and it is possible that some additional fast processes are obscured by the IRF.

(54) Rothe, C.; Monkman, A. *J. Chem. Phys.* **2005**, *123*, 244904.

(55) (a) Isaksson, M.; Norlin, N.; Westlund, P. O.; Johansson, L. B. Å. *Phys. Chem. Chem. Phys.* **2007**, *9*, 1941−1951. (b) Abramavicius, D.; Valkunas, L.; van Grondelle, R. *Phys. Chem. Chem. Phys.* **2004**, *6*, 3097−3105.

(56) Saini, S.; Singh, H.; Bagchi, B. *J. Chem. Sci.* **2006**, *118*, 23−35.

(57) Scholes, G. D. *Annu. Rev. Phys. Chem.* **2003**, *54*, 57−87.

(58) (a) Ulrich, G.; Goeb, S.; De Nicola, A.; Retailleau, P.; Ziessel, R. *Synlett* **2007**, 1517−1520. (b) Goeb, S.; Ziessel, R. *Org. Lett.* **2007**, *9*, 737−740.

(59) Ulrich, G.; Goeb, S.; De Nicola, N.; Retailleau, P.; Ziessel, R. *J. Org. Chem.* **2011**, *76*, 4489−4505.

(60) Bajzer, Z.; Sharp, J. C.; Sedarous, S. S.; Prendergast, F. G. *Eur. J. Biophys.* **1990**, *18*, 101−115.

(61) Moore, A. L.; Dirks, G.; Gust, D.; Moore, T. A. *Photochem. Photobiol.* **1980**, *32*, 691−695.

(62) According to molecular dynamics simulations made with PMEX, the average center-to-center separation between MEBod units is ca. 28 Å, while the mean orientation factor is 1.07. It appears that this branch is less flexible than the lower branches connecting MEBod to TMBod, and this is responsible for the higher interstrand kEET.

(63) Flomenbom, O.; Amir, R. J.; Shabat, D.; Klafter, J. *J. Lumin.* **2005**, *111*, 315−325.

(64) (a) Chemisana, D. *Renewable Sustainable Energy Rev.* **2011**, *15*, 603−611. (b) Currie, M. J.; Mapel, J. K.; Heidel, T. D.; Goffri, S.; Baldo, M. A. *Science* **2008**, *321*, 226−228. (c) Mulden, C. L.; Theogarajan, L.; Currie, M.; Mapel, J. K.; Baldo, M. A.; Vaughn, M.; Willard, P.; Bruce, B. D.; Moss, M. W.; McLain, C. E.; Morseman, J. P. *Adv. Mater.* **2009**, *21*, 3181−3185.

(65) (a) Calzaferri, G. *Top. Catal.* **2010**, *53*, 130−140. (b) Campbell, W. M.; Burrell, A. K.; Officer, D. L.; Jolley, K. W. *Coord. Chem. Rev.* **2004**, *248*, 1363−1379. (c) Poirel, A.; De Nicola, A.; Ziessel, R. *Org. Lett.* **2012**, *14*, 5696−5699.

(66) Bozdemir, C. A.; Yilmaz, M. D.; Buyukcakir, O.; Siemiarczuk, A.; Tutas, M.; Akkaya, E. U. *New J. Chem.* **2010**, *34*, 151−155.

(67) Bura, T.; Leclerc, N.; Fall, S.; Leveque, P.; Heiser, T.; Retailleau, P.; Rihn, S.; Mirloup, A.; Ziessel, R. *J. Am. Chem. Soc.* **2012**, *134*, 17404−17407.

(68) (a) Reisfeld, R. *Opt. Mater.* **2010**, *32*, 880−886. (b) Taleb, A. M. *Renewable Energy* **2002**, *26*, 137−142.

(69) Cerdan, P. D.; Chory, J. *Nature* **2003**, *423*, 881−885.

(70) Hoffmann, S. *Gartenbauwissenschaft* **1999**, *64*, 100−105.

(71) Bradshaw, D. S.; Andrews, D. L. *Polymers* **2011**, *3*, 2053−2077.

(72) Müllen, K. M.; van Stokkum, I. H. M. *J. Statistical Software* **2007**, *18*, 1−46.

(73) Phillips, J. C. *J. Statistical Software* **1996**, *59*, 1133−1207.

(74) Alvarez, F.; Alegria, A.; Colmenero, J. *Phys. Rev. B* **1991**, *44*, 7306−7312.

(75) Curutchet, C.; Scholes, G. D.; Mennucci, B.; Cammi, R. *J. Phys. Chem. B* **2007**, *111*, 13253−13265.

(76) Ghiggino, K. P.; Yeow, E. K. L.; Haines, D. J.; Scholes, G. D.; Smith, T. A. *J. Photochem. Photobiol., A* **1996**, *102*, 81−86.

(77) Englman, R.; Jortner, J. *Mol. Phys.* **1970**, *18*, 145−172.

(78) Liu, D. J.; De Feyter, S.; Cotlet, M.; Stefan, A.; Wiesler, U. M.; Herrmann, A.; Grebel-Kochler, D.; Qu, J. Q.; Müllen, K.; De Schryver, F. C. *Macromolecules* **2003**, *36*, 5918.

(79) Kodriano, Y.; Poem, E.; Lindner, N. H.; Tradonsky, C.; Gerardot, B. D.; Petroff, P. M.; Avron, J. E.; Gershoni, D. *Phys. Rev. B* **2010**, *82*, 155329.

(80) Jordanides, X. J.; Scholes, G. D.; Fleming, G. R. *J. Phys. Chem. B* **2001**, *105*, 1652−1669.

(81) (a) Fron, E.; Schweitzer, G.; Jacob, J.; Van Vooren, A.; Beljonne, D.; Müllen, K.; Hofkens, J.; Van der Auweraer, M.; De Schryver, F. C. *ChemPhysChem* **2007**, *8*, 1386−1393. (b) Larsen, J.; Bruggemann, B.;

Polivka, T.; Sundstrom, V.; Akesson, E.; Sly, J.; Crossley, M. J. *J. Phys. Chem. A* **2005**, *109*, 10654−10662. (c) De Schryver, F. C.; Vosch, T.; Cotlet, M.; Van der Auweraer, M.; Mullen, K.; Hofkens, J. *Acc. Chem. Res.* **2005**, *38*, 514−522.
(82) (a) Nguyen, T. Q.; Martini, I. B.; Liu, J.; Schwatz, B. J. *J. Phys. Chem. B* **2000**, *104*, 237−255. (b) Ruseckas, A.; Ribierre, J. C.; Shaw, P. E.; Staton, S. V.; Burn, P. L.; Samuel, I. D. W. *Appl. Phys. Lett.* **2009**, *95*, 183305.
(83) (a) Khairutdinov, R. F.; Serpone, N. *J. Phys. Chem. B* **1999**, *103*, 761−769. (b) Kelley, R. F.; Goldsmith, R. H.; Wasielewski, M. R. *J. Am. Chem. Soc.* **2007**, *129*, 6384−6385.
(84) (a) Andrews, D. L.; Li, S.; Rodriguez, J.; Slota, J. *J. Chem. Phys.* **2007**, *127*, 134902. (b) Andrews, D. L.; Li, S. *Chem. Phys. Lett.* **2006**, *433*, 239−243. (c) Blumen, A.; Volta, A.; Jurjiu, A.; Koslowskib, T. *Physica A* **2005**, *356*, 12−18. (d) Rana, D.; Gangopadhyay, G. *J. Chem. Phys.* **2003**, *118*, 434−443. (e) Vlaming, S. M.; Heijs, D. J.; Knoester, J. *J. Lumin.* **2005**, *111*, 349−358.